Diverse Causes of Extreme Rainfall in November 2023 over Equatorial Africa

Hermann N. Nana[1]* · Masilin Gudoshava[2] · Roméo S. Tanessong[3,1] · Alain T. Tamoffo[4] · Derbetini A. Vondou[1]

[1]Laboratory for Environmental Modelling and Atmospheric Physics (LEMAP), Physics Department, University of Yaounde 1, PO Box 812, Yaounde (Cameroon)

[2]IGAD Climate Prediction and Applications Centre (ICPAC), Nairobi, (Kenya)

[3]Department of Meteorology and Climatology; Higher Institute of Agriculture, Forestry, Water and Environment; University of Ebolowa, PO Box 118, Ebolowa (Cameroon)

[4]Climate Service Center Germany (GERICS), Helmholtz-Zentrum Hereon, Fischertwiete 1, 20095 Hamburg, Germany

* Corresponding author: Hermann N. Nana (nanahermann100@yahoo.com)

Hermann N. Nana's orcid: https://orcid.org/0000-0002-0973-8613

Masilin Gudoshava's orcid: https://orcid.org/0000-0003-0315-9271

Roméo S. Tanessong's orcid: https://orcid.org/0000-0003-3804-5901

Alain T. Tamoffo's orcid: https://orcid.org/0000-0001-8482-8881

Derbetini A. Vondou's orcid: https://orcid.org/0000-0002-8681-5328

Abstract

Understanding the atmospheric factors that lead to extreme rainfall events is essential to improve climate forecasting. This study aims to diagnose the physical processes underlying the extreme rainfall event of November 2023 in Equatorial Africa (EA), using the ERA5 reanalysis dataset. Composite, spatio-temporal and correlation analyses are used to shed light on the relationship between the November 2023 extreme precipitation events and the various associated factors. The analysis reveals that these extreme rainfall were mainly controlled by several factors that occurred during this period in the Pacific, Atlantic and Indian oceans. These factors include strong Sea-Surface-Temperature (SST) anomalies in Niño-3.4, North Tropical Atlantic, Equatorial Atlantic and Indian Ocean Dipole (IOD) oceanic regions, changes in zonal winds, the Walker circulation, the anomalous moisture flux and its divergence, the easterly jets and the activity of the Madden-Julian Oscillation (MJO). This convergence of moisture flows entered the EA region through its western and eastern boundaries, coming from the equatorial Atlantic and Indian oceans respectively. The juxtaposition of these factors has led to strong and positive rainfall anomalies in EA, with the highest values over the East African region, mainly over southern Ethiopia, Somalia, Kenya and Tanzania, which received more than 430 mm of rainfall during this month. Our findings suggest that many dynamic atmospheric effects need to be taken into account jointly to anticipate this type of extreme event. The results of the present study contribute to the improvement of sub-seasonal to seasonal rainfall forecasts by the region's national meteorological services, to enable us to increase the resilience of the region's citizens to these extreme weather conditions.

Keywords: Equatorial Africa, IOD, atmospheric circulation, SST, rainfall variability

1. Introduction

In recent decades, Equatorial Africa (EA) has experienced an increase in the frequency and intensity of extreme events, particularly droughts, torrential rains and floods (Kilavi et al. 2018). In addition, climate-sensitive sectors such as water, transport, health and agriculture, among others, are negatively impacted by these events, which have recently increased in magnitude and frequency. Flooding from these extreme events leads to infrastructural and socio-economic damage, water shortages, severe human damage and socio-economic disruption (Funk et al. 2008; Tanessong et al. 2017). With the increase in greenhouse gases, the impacts of these extreme events continue and are projected to increase (Gudoshava et al. 2020; Ngavom et al. 2024). East and Central African countries are the regions influenced by high levels of intra-seasonal to inter-annual variability in rainfall (Lüdecke et al. 2021), which are the main flood-prone countries in Africa (Li et al. 2016). These exceptional flooding events generally occur during October and November months, which correspond to rainy months in Central and East Africa (Wainwright et al. 2020; Nicholson et al. 2022; Kenfack et al. 2024).

During November 2023, EA experienced a very wet period during which many parts of the region were affected by extreme rainfall events, most pronounced over East Africa where heavy rainfall and floods caused damage in several countries such as Somalia, Ethiopia, Kenya, Burundi and Malawi (https://floodlist.com/africa/east-africa-floods-november-2023-somalia-ethiopia-kenya-burundi-malawi; Herrnegger et al. 2024), causing up to 90 deaths and more than 113,690 temporarily displaced. In Kenya, many areas were devastated by significant flooding. At least 19 of the country's 47 counties were severely affected by the floods, which started at the end of October 2023. More than 46 people lost their lives and over 58,000 people have been displaced by the increased heavy precipitation and subsequent flooding (https://floodlist.com/africa/kenya-floods-update-november-2023). In Tanzania, some 10,090 people, or 2,018 households, were affected, and 1,245 houses were damaged, with over 40 deaths recorded (https://floodlist.com/africa/tanzania-floods-landslides-hanang-district-december-2023). Extreme rainfall events also occurred in western EA regions. Democratic Republic of the Congo (DRC), Central African Republic (CAR) and Nigeria countries also experienced significant flooding and landslides which affected over 90,000 people, and around ten schools and health centres were destroyed (https://www.unocha.org/publications/report/burkina-faso/west-and-central-africa-weekly-humanitarian-snapshot-15-21-november-2023). These conditions have placed EA in a severe food crisis. Given that climate models project a trend of increased extreme rainfall in the region (Fotso-Ngeumo et al. 2019), and that the impacts of these extreme events are expected to increase (Gudoshava et al. 2020), it is therefore essential to understand the processes behind these extreme events.

Numerous studies have examined the different causes of November's extreme rainfall in the EA. They have shown that these extreme events were associated with numerous mechanisms linked to Sea-Surface-Temperature (SST) patterns in the tropical Pacific, Atlantic and Indian Oceans (Nana et al. 2023, 2024; Palmer et al. 2023; Roy and Troccoli 2024). These large-scale ocean drivers are the El Nino-Southern Oscillation (ENSO;

Palmer et al. 2023), Indian Ocean Dipole (IOD; Nicholson 2015; Roy and Troccoli 2024), North Tropical Atlantic (NTA; McHugh and Rogers 2001; Ingeri et al. 2024) and the Equatorial Atlantic (ATL; Dezfuli and Nicholson 2013). Studies by Nicholson (2015) showed that IOD plays a role in the East African rainfall modulation, while Palmer et al. (2023) showed that increased rainfall in this region is due to the presence of positive IOD events during the October-December (OND) season. Following Wahiduzzaman and Luo (2020), several IOD episodes coincide with an ENSO event, and Zhang et al. (2015) found that an ENSO episode can lead to the development of an IOD event through the Walker circulation that connects the Indian and Pacific Oceans. In this line, Roy and Troccoli (2024) have shown that the increase in rainfall over East Africa is linked to the simultaneous presence of two factors, the IOD and ENSO. Moihamette et al. (2022) conducted a similar study but focused on the months of September-October-November over Central Africa. They found that during this period, the warm (positive IOD with El Niño) and cold (negative IOD with La Niña) phases of the IOD and ENSO frequently coincide. This study also showed that positive IOD events contribute significantly to more rainfall in Central Africa after the El Niño effect is removed. Another driver of East African rainfall is the NTA, which conducts more rainfall over many countries, mainly Tanzania, Kenya and Uganda (Ingeri et al. 2024). Over western EA, the Indian Ocean influences the climate system of this region through the ATL region, mainly in October and November (Moihamette et al. 2024). Furthermore, in November, ENSO and IOD were not considered to be important factors in many flood-affected regions, particularly northern regions (north of 5° N; e.g. Moihamette et al. 2022). Consequently, all the events of November 2023 were probably the result of the simultaneous occurrence of several factors. These include SST in the Indian, Atlantic and Pacific oceans, the atmospheric zonal circulation, Walker circulation, Madden-Julian Oscillation (MJO; Madden and Julian 1971, 1972) activity, moisture transport and divergence and African Jets.

This study aims to identify and analyse the different factors that can sustain these extreme rainfall events in Equatorial Africa. This paper is structured as follows: Data and metrics used to diagnose mechanisms are described in Section 2 and features in the EA rainfall and ocean SSTs are presented in Section 3. Physical processes and underlying mechanisms associated with rainfall extremes are shown in Section 4. Section 5 summarizes and concludes the document.

2. Data and Methods

2.1. Data

ERA5 produces monthly estimates of climate variables on a global scale, featuring a horizontal resolution of 31 km (0.25° x 0.25°) and 137 vertical levels ranging from the surface to 1 hPa (Hersbach et al. 2020) available from 1979 through the present. In this study, we extracted ERA5 monthly data for rainfall (precip in mm day^{-1}), SST (sst in K), zonal and meridional winds (u and v in m s^{-1}), specific humidity (q in kg kg^{-1}), vertical velocity (w in Pa s^{-1}), surface pressure (sp in Pa), total column water vapor (tcwv in mm) , 2-meter dew point temperature (d2m in K), surface net solar radiation (ssr in J m^{-2}) and low cloud cover (lcc in %). The data span 23 vertical levels, from 1000 to 200 hPa, and cover the period from November 1981 to 2023. To assess the ability of ERA5 to reproduce rainfall

extremes that occurred in November 2023, the observational dataset from the Climate
Hazards Group InfraRed Precipitation with Station dataset (CHIRPS; Funk et al. 2015) is
used. This dataset includes high-resolution satellite imagery and station rain-gauge data,
available from 1981 through the present and has a high spatial resolution of 0.05° × 0.05°.
The SST dataset used in this paper to analyse the oceanic conditions is provided by the
Extended Reconstructed Sea Surface Temperature Version 5 (ERSSTv5; Huang et al. 2017).
The dataset is available from 1854 through present at a resolution of 2.0° × 2.0°.

2.2. Methods

The atmospheric factors explored in this study include the DMI, zonal winds, the
Walker circulation over EA and the Oceans, moisture flux and divergence fields, tropical
SSTs in the Pacific, Atlantic and Indian Oceans, and tropical waves, namely African Easterly
Waves and the Madden-Julian Oscillation (MJO). We are focusing on these factors because
they represent the main contributors to extreme rainfall events in the EA (Kuete et al.,
2019; Nicholson et al. 2022; Roy and Troccoli 2024; Gudoshava et al., 2024). The DMI is
calculated as the difference between SST anomalies in a western (60° E-80° E, 10° S-10° N)
and an eastern sector (90° E-110° E, 10° S-0° S) of the central Indian Ocean. Since several
oceans were anomalous during these extreme events, oceanic conditions of additional
regions have been analysed. These are: the North Tropical Atlantic (NTA; 5°-15° N and 40°-
15° W), the Equatorial Atlantic (ATL; 3° S-3° N and 20° W-10° E) and the Niño-3.4 (5° S-5° N
and 170°-120° W).

We start our analyses by characterizing rainfall distribution as shown by both
CHIRPS and ERA5 over EA (defined as 10° S-10° N; 10°-50° E, see red box in Figure 1).
Afterwards, processes associated with November anomaly patterns are diagnosed. We
first look at November anomalies in SSTs and specific humidity on the one hand, and then
anomalies in wind and moisture flux, on the other. The zonal and meridional circulation
can be modulated by variations in winds and specific humidity, which can have an impact
on the regional hydrological cycle, either by enhancing or weakening it, following the
findings by Seager et al. (2010) and Tamoffo et al. (2024).

We have also investigated the water vapor mass transported within the zonal
circulation by estimating the zonal mass-weighted stream-functions (Ψ_Z; Stachnik and
Schumacher 2011; Taguela et al. 2022), following the Equation 1:

$$\Psi_Z(\text{p}) = \frac{2\pi R}{g} \int\limits_{sp}^{P\,top} [u]\ \text{dp} \qquad\qquad (1)$$

where R is the Earth's radius (m), g is the constant of gravity, sp and $P\,top$ the surface and
top-level pressure respectively, and bracket terms denote the meridionally averaged of
the zonal wind over the latitudes 10° S-10° N.

Research indicates the existence of a shallow, zonal overturning circulation over
western EA, identified and termed the Congo Basin cell (CB cell) by Longandjo and Rouault
(2020). This cell is a closed, and shallow zonal circulation confined to the lower
troposphere (1000-800 hPa), and remains active throughout the year. Similar to Low-level

196 westerlies (LLWs), the CB cell's intensity and width are influenced by near-surface
197 temperature warming over both the western EA landmass and the eastern equatorial
198 Atlantic (Longandjo and Rouault 2020; Taguela et al. 2022). The cell reaches its peak
199 intensity and width in September. According to Longandjo and Rouault (2020), the CB
200 cell's eastern boundary aligns with the Congo Air Boundary, a convergence zone. Here,
201 LLW originating from the equatorial Atlantic, after traversing western EA, converges with
202 the easterly winds of the Indian monsoon system, creating the cell's ascending branch.
203 This convergence zone is characterized by peak convection and precipitation.
204 Consequently, the longitudinal position of maximum rainfall in the region is determined
205 by the width of the CB cell. Note that the CB cell is characterized by the negative values of
206 the zonal mass-weighted stream-function ($\Psi_z < 0$). This function is used to characterise the
207 Walker-type circulation over the Western EA (Longandjo and Rouault 2020; Tamoffo et al.
208 2022). Environmental conditions for November 2023 are also analysed through an
209 assessment of vertically integrated moisture transport. Vertically integrated moisture flux
210 (Q; Zheng and Eltahir 1998) is calculated using Equation 2 given as follows:

211
$$\vec{Q} = \frac{1}{g} \int_{sp}^{P\,top} q\,\vec{V}\ \mathrm{dp} \qquad (2)$$

212 where $\vec{V}$ is the horizontal wind (m s^{-1}).

213   For all metrics used in this study, composite anomalies are obtained by removing
214 the 42-year average of the period 1981-2022. For significance testing, the student's t-test
215 is applied.

3. Rainfall in November 2023

217   Figure 1 shows the percentage contribution of November rainfall climatology to
218 total annual rainfall (Fig. 1a,d), November mean rainfall (Fig. 1b,e), and the difference
219 between November 2023 and the long-term Mean (LTM) November rainfall (1981-2022;
220 Fig. 1c,f). In general, November 2023 was exceptionally wet throughout the EA, with more
221 rainfall over the eastern Africa area, where monthly anomalies were typically up to 7 mm
222 day^{-1} than that occurring over the western area (Fig. 1c,f). Fig. 4a features Indices of
223 standardised rainfall anomalies over EA since 1981, based on both CHIRPS and ERA5
224 dataset. Extreme positive rainfall anomalies occurred in 1982, 1994, 1997, 2006 and 2019
225 in most parts of equatorial Africa. November 2023 is the strongest since 1981.

226   Positive anomalies prevail from South Sudan and Ethiopia, around 10 to 15° N, to
227 at least 10° S over the eastern region, and over northern (equator to 15° N) and southern
228 (15° S to 5° S) regions, over the western EA area in CHIRPS data (Fig. 1c). There is generally
229 good agreement between ERA5 and CHIRPS except in Congo Republic, northern part of
230 Gabon and central part of DRC, where ERA5 does not well estimate the negative rainfall
231 anomalies (Fig. 1f), and in eastern Africa regions, where ERA5 shows weaker rainfall than
232 CHIRPS. During this month, most parts of the EA region received increased rainfall of up
233 to 2 mm day^{-1}. These areas (except the northern regions) coincide with those that strongly
234 contribute to the annual EA rainfall (Fig. 1a,d) and normally receive at least 3 mm day^{-1} of

total rainfall (Fig. 1b,e). In the typically dry northern regions during November, rainfall ranged between 3 and 9 mm day^{-1}, exceeding the long-term mean (LTM) by approximately 2 to 8 mm day^{-1}.
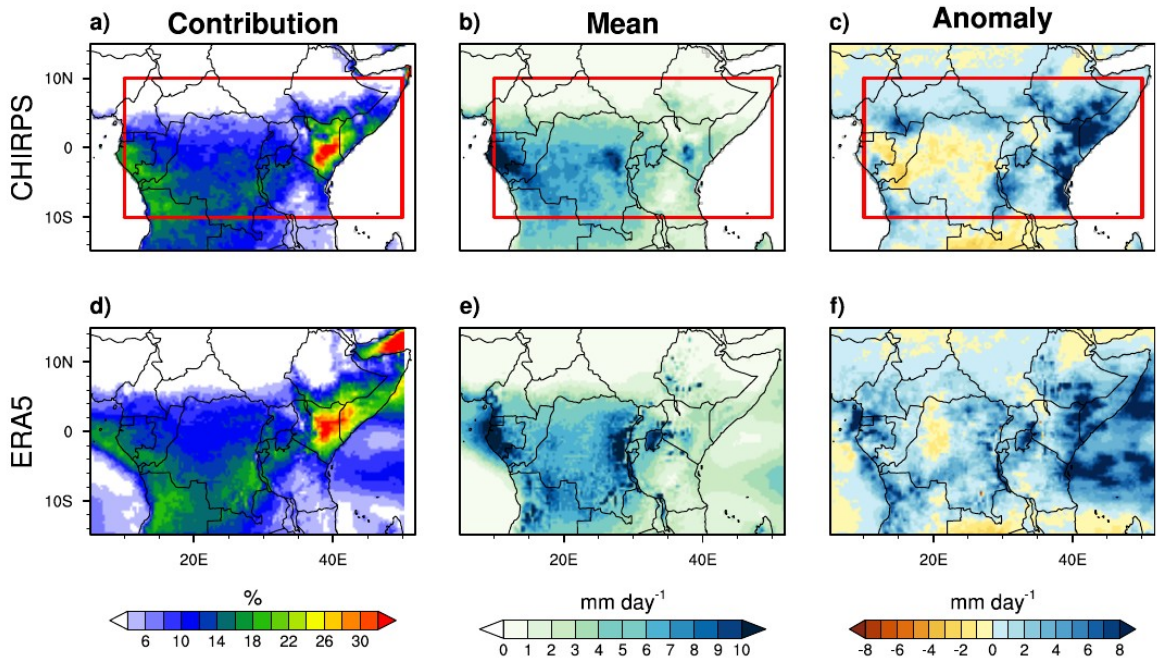
Fig 1: (a, d) Percentage contribution of November climatology to total annual rainfall over tropical Africa, (b, e) LTM (1981-2022) November rainfall and (c, f) November rainfall anomalies. Rainfall anomalies are calculated as the difference between CHIRPS 2023 and CHIRPS LTM November rainfall. The red box indicates the EA region.

4. Identifying important drivers of extreme November 2023 rainfall

4.1. Sea Surface Temperatures

The tropical SST anomalies for November 2023, as estimated by ERSST and ERA5, are shown in Fig. 2. In both datasets, SST anomalies were predominantly positive throughout the equatorial and subtropical regions of the Pacific and Atlantic Oceans. Pacific anomalies were strong and positive over the equator, where anomalies were on the order of 2 to 2.9 K. That, and the positive and significant correlations with SSTs in Niño-3.4 (black box in Fig. 3c) indicate that ENSO was a factor in the East African rainfall anomalies of November 2023 (Chobo and Huo 2024). This ENSO observation occurs when the Indian Ocean features a strong dipole pattern, with positive anomalies in the west pole (10° S-10° N and 50°-70° E) and negative in the east pole (10° S-0° and 90°-110° E). Many studies show that positive ENSO phases are usually associated with positive rainfall anomalies over East Africa (Indeje et al. 2000; Shilenje and Ogwang 2015; Onyutha 2016). However, during the two positive El Niño events, 1983 and 1992, East African countries experienced significant droughts (Shisanya 1990; Ibebuchi 2021). These previous studies

261 also found that in addition to ENSO, IOD plays an important role in the modulation of
262 precipitation in East Africa. During these two years, IOD was in its negative phase. This
263 shows that it is important to take into account the combined influence of ENSO and IOD in
264 the modulation of precipitation over East Africa before and during the OND season. In this
265 line, a recent study by Roy and Troccoli (2024) showed that when IOD and ENSO are both
266 positive in July-August-September (JAS) and OND, this leads to an increased rainfall over
267 East Africa in OND. Note that in JAS 2023, these two modes were in their positive phase
268 (https://origin.cpc.ncep.noaa.gov/products/analysis_monitoring/ensostuff/ONI_v5.php;
269 https://ds.data.jma.go.jp/tcc/tcc/products/elnino/iodevents.html). An important remark is
270 the similar patterns in Niño-3.4, IOD, NTA and ATL areas with those in October-November
271 2019, which were also associated with increased rainfall over East Africa (Nicholson et al.
272 2022; Ingeri et al. 2024).
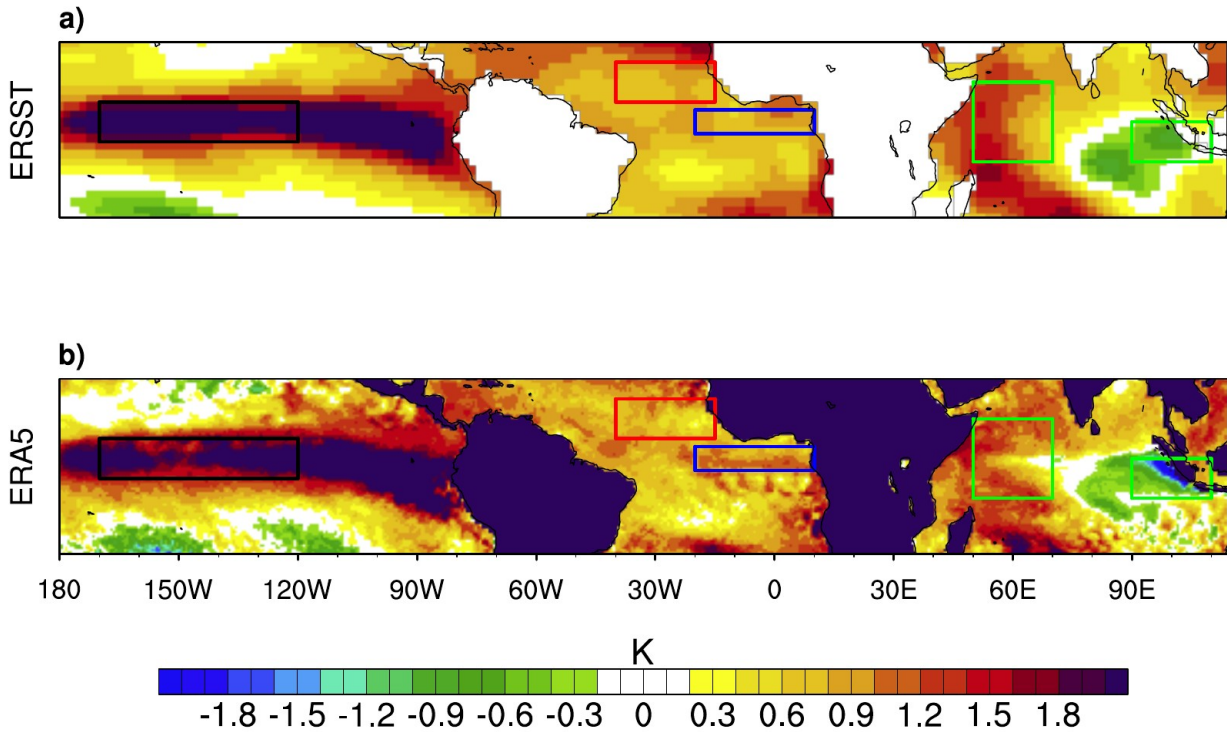
274 **Fig 2:** SST anomalies during November 2023 for (a) ERSST and (b) ERA5. Red and blue boxes
275 indicate the areas for north tropical Atlantic (NTA; 5°-15° N and 40°-15° W) and equatorial Atlantic
276 (ATL; 3° S-3° N and 20° W-10° E) SST calculations, green boxes indicate the areas for DMI
277 calculation. The black box over the Pacific Ocean is Niño-3.4 (5° S-5° N and 170°-120° W).
278

279   Extreme positive values were recorded in November 1997, 2006, and 2019, all of
280 which were exceptionally wet years in eastern EA. The 2023 positive dipole event ranks as
281 the third strongest for November since 1981. Notably, the DMI magnitude in 2023 was
282 smaller than in both November 1997 and 2019, when conditions in EA were considerably
283 drier than in 2023, suggesting that additional factors may have contributed, such as the
284 Niño-3.4, which was absent in 2019 but present in 2023. The event may have influenced

the CB, as significant correlations between the DMI and rainfall are evident (Fig. 3b), with the strongest impact observed in the far eastern EA region (Dezfuli and Nicholson, 2013). However, rainfall anomalies within CB exhibit both positive and negative values, which can be linked to the IOD due to significant correlations over the IOD regions. While heavy rainfall in both CB and eastern Africa is likely associated with the IOD, this does not hold true for other affected areas. Following Dezfuli and Nicholson (2013), correlations between SST and rainfall suggest that November rainfall in western EA is not influenced by the IOD, a conclusion further reinforced by the correlations in Fig. 3c.
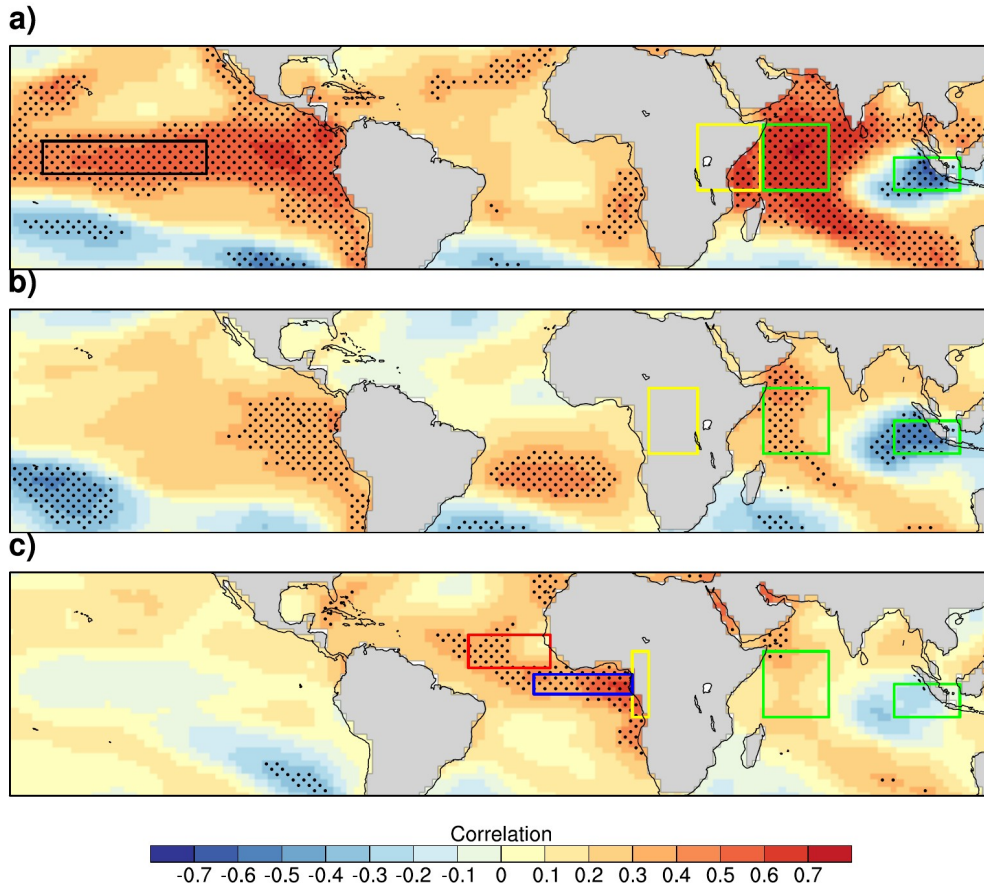
Fig 3: Correlation coefficient between (a) Eastern EA (yellow box; 30° E-50° E), (b) Congo Basin (yellow box; 15° E-30° E), and (c) Western EA (yellow box; 10° E-15° E) rainfall with SST during 1981-2023 period. The oceanic boxes are the same as those in Fig. 2. The stippling occurs where the correlation is statistically significant at the 95% confidence level through the Student's t test. The SST and rainfall data come from ERSST and CHIRPS, respectively.

The intense rainfall in western EA can likely be attributed to the Atlantic SST anomalies. It is important to highlight that SSTs along the eastern Atlantic coast and in the central equatorial Atlantic show a strong positive correlation with November rainfall in western EA, as reported by Lutz et al. (2014). Figure 3c shows correlations of western EA November rainfall with SSTs. Over the Atlantic Ocean, significant and positive correlations

between western EA rainfall and SST occur over NTA, ATL and eastern Atlantic coastal regions (Fig. 3c). Moihamette et al. 2024 suggest that in November, the Atlantic Ocean has a significant influence during positive IOD events, induced by its teleconnection with the Indian Ocean. This is characterized by anomalous westerly winds over the central equatorial Atlantic Ocean (ATL, blue box in Fig. 3c), generating moisture advection towards western EA. These winds originate from the NTA domain (red box in Fig. 3c). Furthermore, these ocean regions feature strong standardised SST anomalies in 2023 (Fig. 4b). A feature to note is the exceptional warmth of SSTs in November 2023 over the NTA area (red line in Fig. 4b). Over the 1981-2023 period, the 2023 anomalies were the warmest on record. Another feature of NTA variability is its positive correlation ($r > 0.2$) with eastern EA rainfall (Fig. 3a). A recent study by Ingeri et al. (2024) showed that positive SST anomalies in NTA from October to December lead to enhanced East African rainfall, mainly over Tanzania, Kenya and southern Uganda. In addition, the SST time series over the equatorial Atlantic showed that the 2023 anomalies were the second warmest year after the November 2019 anomalies which led to a significant increase in rainfall over western EA (Nicholson et al. 2022; Kenfack et al. 2024).

The time series of SSTs for the Niño-3.4 region over the period 1981-2023 (black line in Fig. 4c) indicates the warmth in November 2023. During this period, the 2023 anomalies ranked among the three warmest years on record. This Pacific sector exhibits the strongest correlation with November rainfall over the CB (Moihamette et al. 2022) and over eastern EA (Fig. 3a; Palmer et al. 2023; Chobo and Huo 2024; Roy and Troccoli 2024). These SST anomalies likely played a key role in the positive rainfall anomalies observed in eastern EA, especially in coastal areas, as well as in the CB. Roy and Troccoli (2024) showed that when IOD and ENSO are both positive in November, this contributes to excessive rainfall over the whole of East Africa, south of the DRC, north of Angola, Nigeria and CAR, while deficit rainfall occurs over certain parts of DRC. In this line, the study by Moihamette et al. (2022) showed that during simultaneous both positive IOD and ENSO events, the influence of the positive phase of IOD on EA rainfall is significant with the non-El Niño effect and this is characterized by an increase in moisture advection toward EA that contributes to an enhancement of rainfall intensity, more pronounced over eastern and western EA.
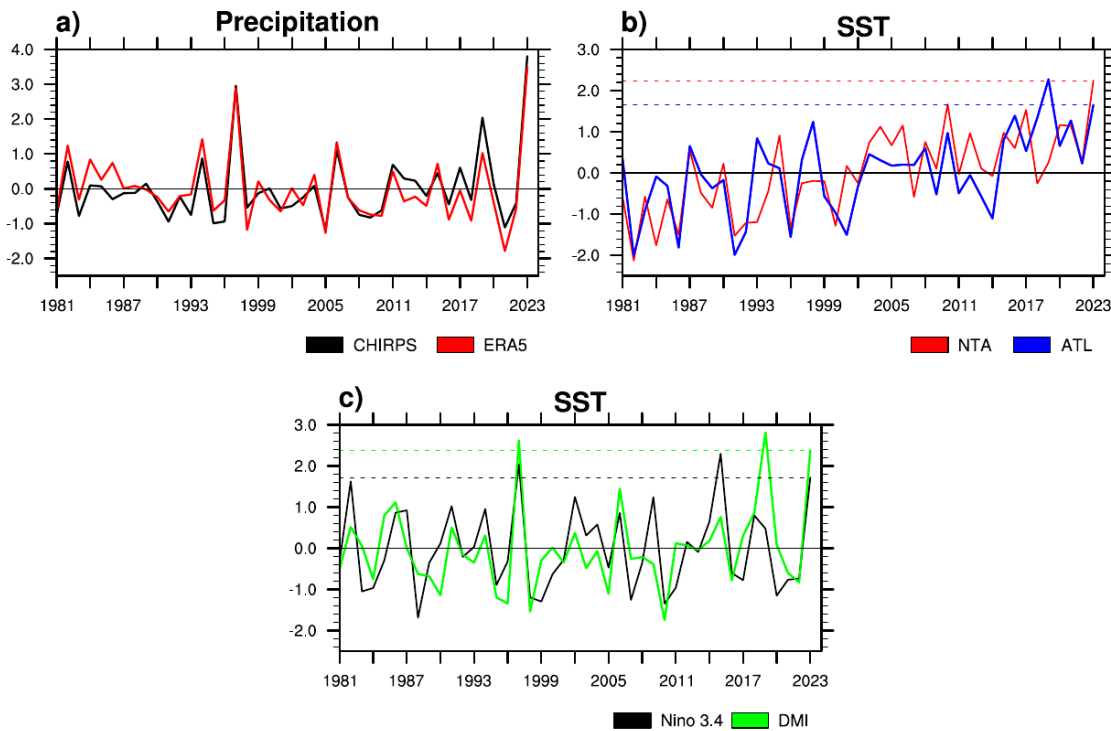
Fig 4: (a) Indices of standardised rainfall anomalies over 1981-2023, averaged over the red box indicated in Fig. 1. (b) Indices of standardised SST anomalies over 1981-2023, average over the NTA and ATL oceanic regions. (c) As in (b), but for the DMI and ENSO index averaged over the IOD and Niño-3.4 oceanic regions. The SST data come from ERSST. The dotted horizontal lines on maps (b) and (c) indicate values for the year 2023.

4.2. Dynamic factors associated with the November 2023 extreme rainfall

Many studies (eg., Pokam et al. 2012, 2014; Taguela et al., 2022) proposed a physical mechanism for modulating the long rains over CB on interannual timescales. They identified that changes in the low-level westerlies (LLW) over the equatorial Atlantic Ocean play a significant role in this modulation. These westerlies influence the moisture transport and atmospheric conditions over the region (Nana et al. 2023), impacting the onset, intensity, and duration of the long rains. Variations in LLW can alter the regional climate patterns, and this mechanism helps explain the variability of the long rains in relation to other climatic phenomena, such as the ENSO.

The maximum moisture convergence over equatorial central Africa in SON is found to be a consequence of low-level moisture advection from the Atlantic Ocean. These LLWs are controlled by the heating contrast between land and ocean (Pokam et al. 2014). These heating contrasts lead to a Walker-type circulation over the Atlantic Ocean and equatorial central Africa with the development of LLW as its lower branch. These LLW over the equatorial Atlantic are strongly correlated with DMI (Moihamette et al. 2024). For East Africa rainfall variability, numerous studies have identified ENSO and IOD as the two main atmospheric drivers that influenced the October-November-December (OND) rainfall (Indeje et al. 2000; Shilenje and Ogwang 2015; Roy and Troccoli 2024). Following Black

361 (2005), these drivers play an important role in the moisture convergence over East Africa
362 through moisture advection from the Indian Ocean, even if they are not independent of
363 each other. Roy and Troccoli (2024) showed that when ENSO and IOD are in the same
364 phase during JAS, the Walker-like circulation appears to play a major role in modifying the
365 ascending branch into a descending branch in two situations (positive and negative
366 phases) during OND period.

367 **4.2.1. Zonal circulation/winds, Walker circulation and water vapor mass transported**
368 **over tropical Oceans**
369

370 Following the recent study of Longandjo and Rouault (2024), rainfall variability over
371 EA is highly dependent on moisture inputs linked to atmospheric circulation. It is
372 therefore important to show the characteristics of these moisture inputs to identify their
373 oceanic origin.

374 Figure 5 depicts the vertical profile of specific humidity (first row) and zonal
375 moisture flux (shaded) overlaid by zonal wind (contour; second row) in November for the
376 climatology of 1981-2022 (Fig. 5a,d), 2023 average (Fig. 5b,e) and the anomaly (Fig. 5c,f),
377 averaged between 10° S-10° N.

378 Over the Indian Ocean, the 1981-2022 climatology is characterized by intense
379 westerly flux, whereas the November 2023 average appears to be an easterly flux (Fig.
380 5d,e). Over the continent, moisture flux is predominantly easterly or westerly during
381 November 2023 as in the climatology. We can conclude from this that two distinct
382 mechanisms govern the moisture flux over the Indian Ocean and the continent. It is
383 noteworthy that the anomaly analysis (Fig. 5c) confirms that there was more moisture
384 over the EA in November 2023 than in the 1981-2022 climatology. This moisture surplus
385 appears here to extend up to 400 hPa and is more pronounced over eastern EA between
386 900 and 500 hPa.

387 In addition, from the Atlantic Ocean, the westerly wind in 2023 was more
388 pronounced near 30° E compared to the climatology (near 17° E). These results lead to a
389 strong moisture flux from the Atlantic (Indian) Ocean over western (eastern) EA (Fig. 5f),
390 following the work of Chadwick et al. (2016) who showed that increased humidity over
391 land would be a response to increased moisture advection from the oceans under
392 warming. The easterly flux over eastern EA is strong at the middle troposphere, where
393 strong moisture is observed. It is interesting to note that the intensity of the LLW
394 anomalies appears to extend to the upper troposphere (mainly 300 hPa). In conclusion,
395 the intensification of the zonal wind over EA indicates that this moisture (strong from 900
396 hPa) probably comes from both the equatorial Atlantic and Indian Oceans.
397
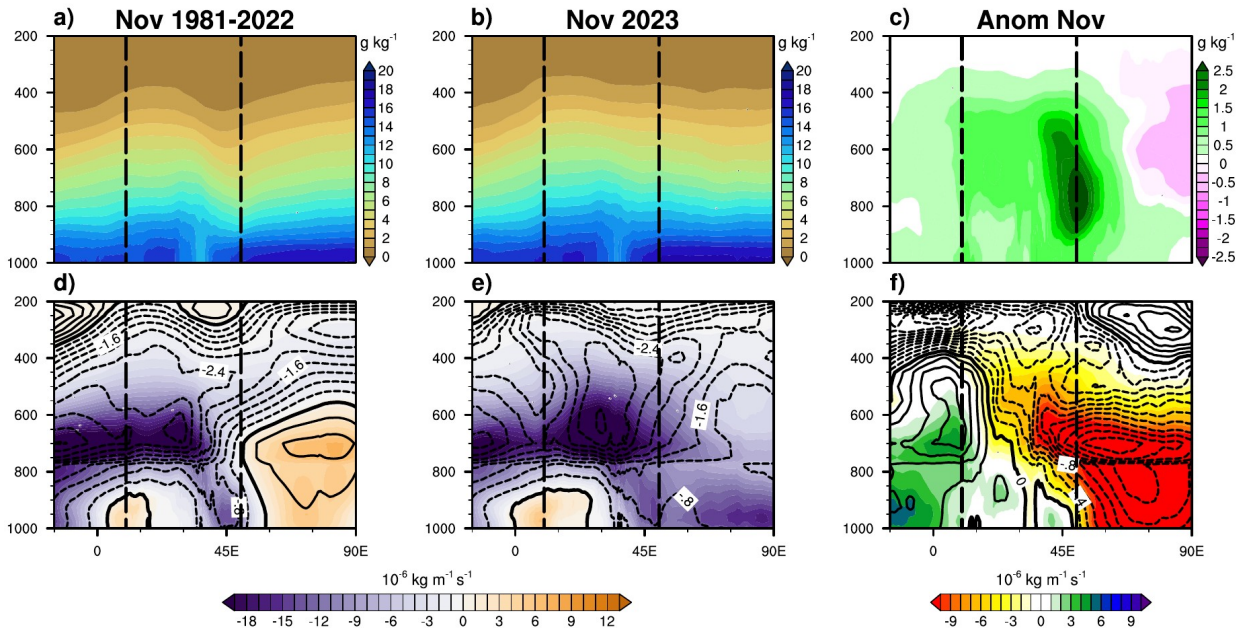
Fig 5: Longitude-height cross-sections of (first row) specific humidity and (second row) zonal moisture flux (shaded: 10^{-6} kg m^{-1} s^{-1}) and zonal wind (contour: m s^{-1}) for (a,d) the climatology of November 1981-2022, (b,e) November 2023 and (c,f) the anomaly, averaged between 10° S-10° N. The dashed black lines denote the limits of EA.

The precedent anomaly analysis leads us to conclude that both the Atlantic and Indian oceans contribute to the moisture increase (so more rainfall in November 2023) over the EA and that ENSO has a possible contribution mainly over the eastern EA. This suggests large-scale tropical climate control. To examine the links with tropical circulation, large-scale wind, omega and water vapor mass transported field analyses are carried out, and the results are present in Figures 6-9.

From the lower to the high troposphere, anomalous westerly (easterly) winds across the equatorial Atlantic (western Indian) region penetrate the EA domain through its western (eastern) border (Fig. 6a-c). These westerly winds come from the NTA region (at the low troposphere, Fig. 6a). Over eastern EA, the heavy rains of November 2023 were accompanied by a weakening of the westerly winds and reduced subsidence in the Indian Ocean, resulting in a supply of moisture to the continent (Hastenrath et al. 2010, 2011).
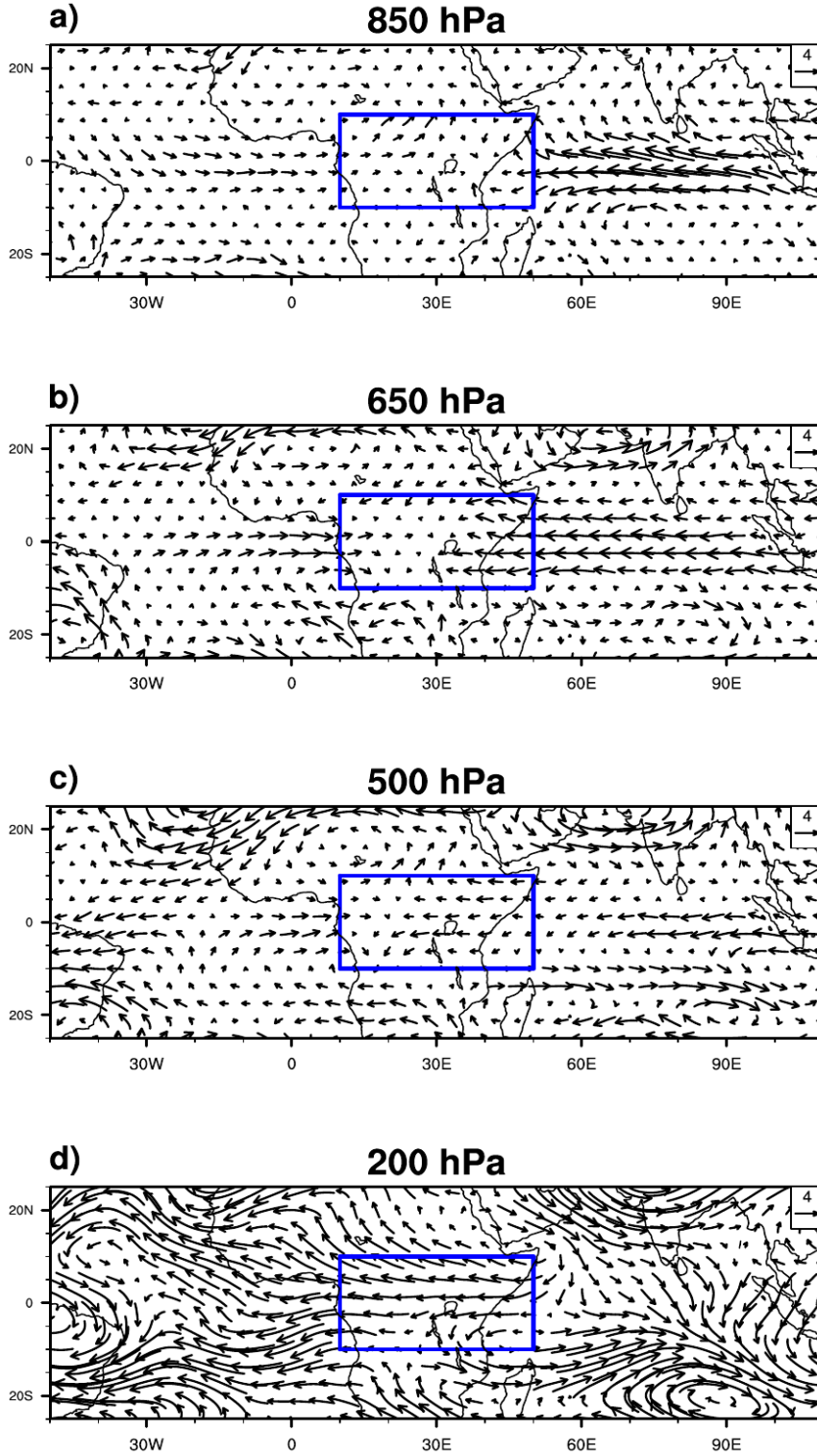
Fig 6: Vector wind (m s⁻¹) anomalies (Nov. 2023 minus 1981-2022 mean) at (a) 850 hPa, (b) 650 hPa, (c) 500 hPa and (d) 200 hPa. The blue box indicates the EA region.

In addition, over both the equatorial Pacific and Atlantic Oceans, and western EA, westerly anomalies feature at 850 hPa while easterly anomalies are evident over the equatorial Indian Ocean (Fig. 7c). Inverse anomalies are observed at 200 hPa (Fig. 7b), suggesting that the west-east zonal circulation is subject to changes. These later are

shown by the upper-level divergence and vertical motion analysis. Equatorial Africa and the coasts of the Atlantic and Indian Oceans feature strong divergence at 200 hPa, followed by strong convergence over the NTA and eastern Indian Ocean regions (Fig. 7a), the reverse divergence anomalies' pattern characterises lower-troposphere level (not shown). These patterns are consistent with Walker circulation, which has been examined by both vertical velocity (omega), and zonal wind combined with vertical velocity (Fig. 8). Note that negative values of omega denote ascent motions and positive values indicate subsidence.
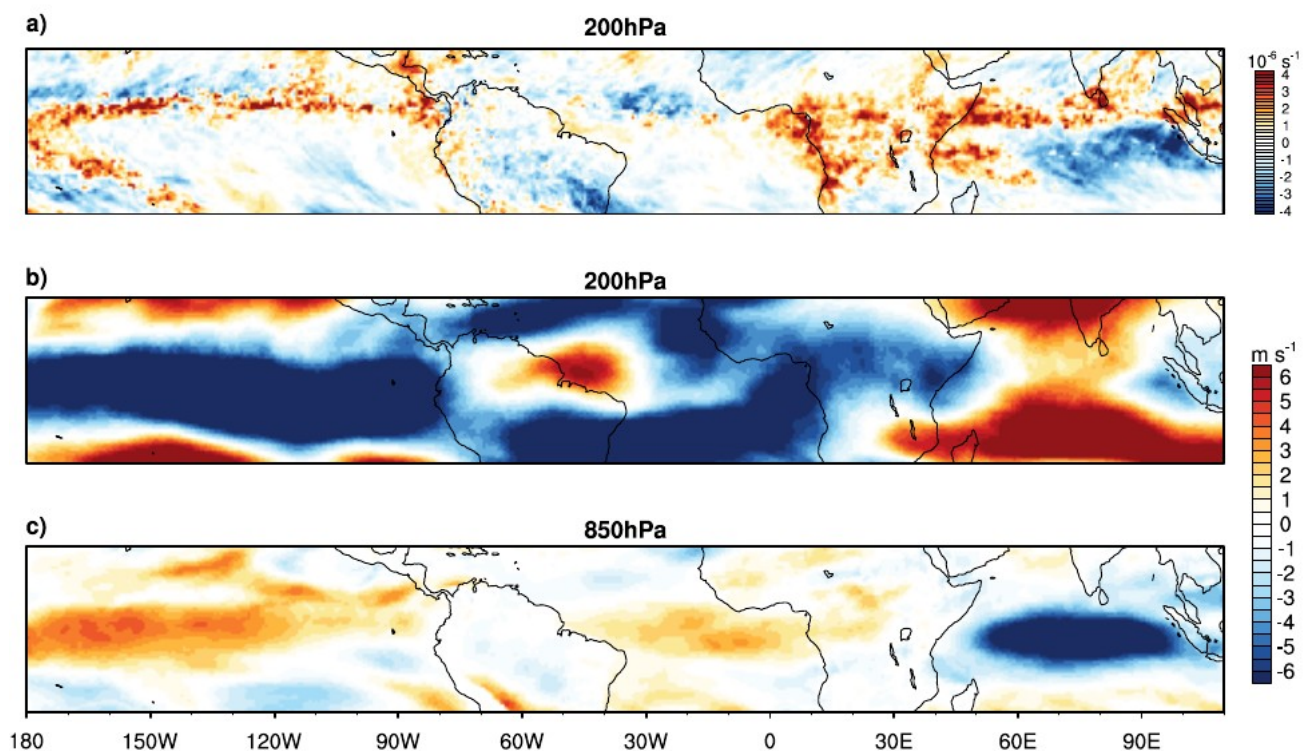
Fig 7: Anomalies of (a) divergence (10^{-6} s^{-1}) at 200 hPa and zonal wind (m s^{-1}) at (b) 200 hPa and (c) 850 hPa.

For the 1981-2022 climatology (Fig. 8a), Omega indicates that the ascent motions of the Indian Ocean Walker cell are very pronounced. The western Atlantic Ocean is characterized by strong rising motions, while the eastern Atlantic Ocean experiences sinking motions. Over western Africa (10° E to 30° E), the entire atmospheric column shows significant upward motion, whereas in eastern Africa (30° E to 45° E), rising motions dominates at low levels, while sinking motions prevails in the mid- and upper troposphere. This subsidence in eastern Africa leads to reduced rainfall. These findings are consistent with those observed during the exceptional October/November 2019 events, as noted by Nicholson et al. (2022). By contrast, these branches are weak in general during November 2023 (Fig. 8b). In contrast to climatology, 2023 shows strong ascendance at mid- and upper-troposphere over eastern Africa. Here, we focus on three omega (color), and zonal wind combined with vertical velocity (vector) patterns to evaluate

the location and strength of the African Walker circulation cells. Anomalous rising motion corresponds to areas with low-level converging vectors, mid-level ascent motions and upper-level diverging vectors that will typically experience more rainfall. Following Fig. 8c, at 850 hPa, anomalous rising (sinking) motions are associated with areas of westerly (easterly) anomalies. At 200 hPa, anomalous ascendance (subsidence) corresponds to areas of easterly (westerly) anomalies.

It is noteworthy that rainfall deficits are observed over the Congo Basin, around 15-35° E. This region of rainfall deficits is linked to a corresponding area of reduced rising motion at low levels (Fig. 8c). Over the three oceans, the zonal cells are weaker, but more pronounced over the Atlantic and Indian oceans than the Pacific ocean. In the case of the Pacific Ocean, the increase of Pacific cells is linked with the El Niño events and are moved westward and vertical motion anomalies are weak along the coast of South America. Thus, the SST's El Niño pattern could be highly developed. Both the Atlantic and Indian Oceans feature greater vertical motion contrasts than the Pacific Ocean. This is characterised by an increased ascent (subsidence) over the eastern and western Atlantic and Indian oceans respectively, and increased subsidence (ascent) over the western and eastern Atlantic and Indian oceans respectively. The consequence is a strengthening of the ascent which extends over equatorial Africa and is accompanied by an increase in rainfall over Africa, mainly in East Africa.
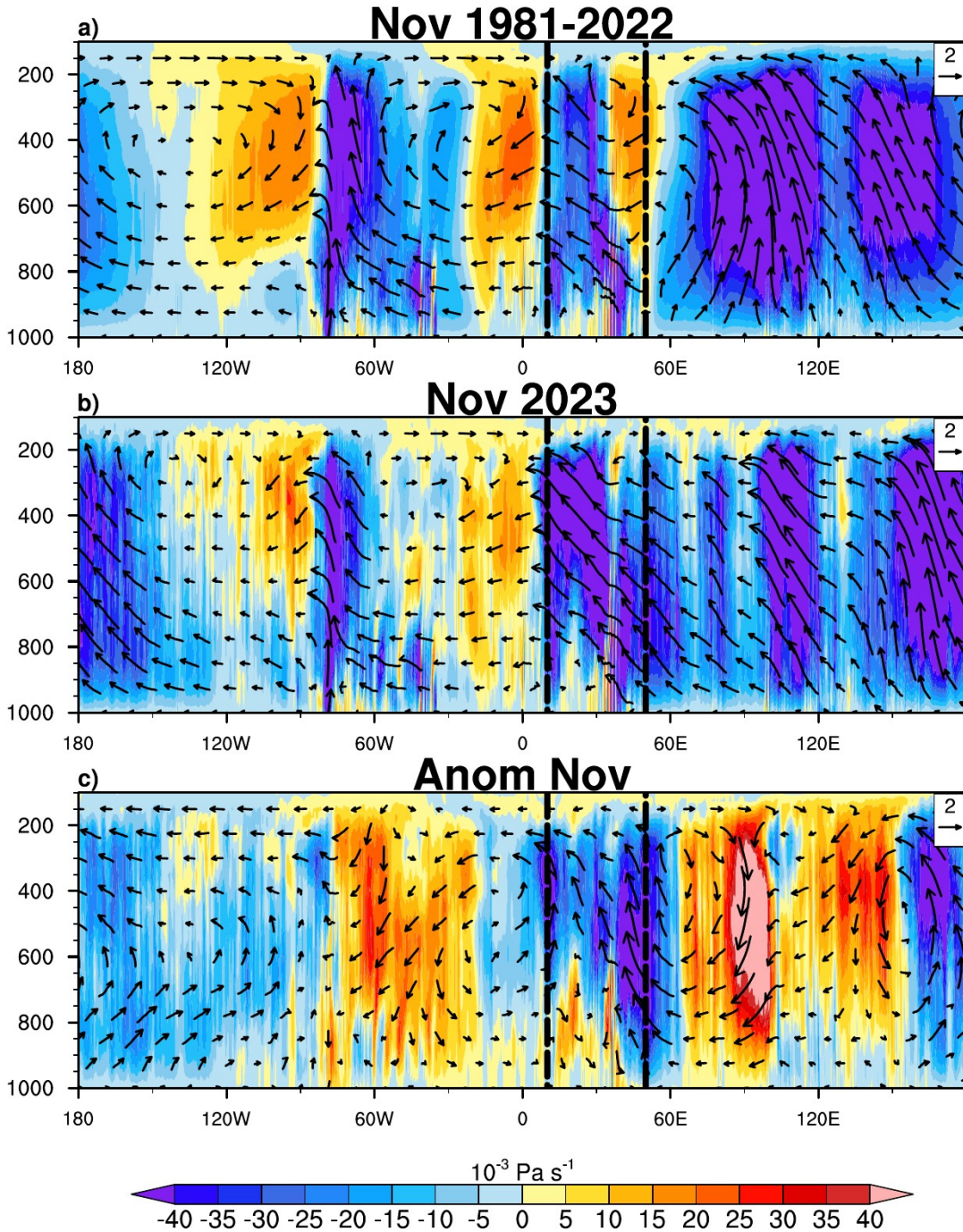
Fig 8: Longitude-height cross-sections of vertical velocity (Omega: 10^{-3} Pa s^{-1}) selected over latitude 10° S-10° N in November for (top to bottom) climatology, November 2023, and anomaly. The shading (background) represents the vertical velocity, with negative values denoting ascent motions and positive values indicating subsidence. Additionally, the vectors (overlay: m s^{-1}), obtained with the zonal wind component and vertical velocity, illustrate the behavior of the air mass during upward or downward movements. The dashed black lines denote the limits of EA.

To further investigate the vertical motion, the water vapor mass transported analysis is done through the mass-weighted stream-function (Fig. 9). In the climatology mean (Fig. 9a), the CB cell ($\psi < 0$) is located between 1° and 18° E and extends up to 950

hPa, whereas it occurs at -1 and 28° E and extends around 975 hPa during November 2023 (Fig. 9b). These CB cell locations coincide with the Walker cell ascending branch (Fig. 8a,b) over EA, more intense during November 2023 associated with sinking branches over the Equatorial Atlantic and Indian Oceans (Figs. 8c and 9c). Near to 800 hPa, the westward ($\psi > 0$) of the circulation is greater during November 2023 (Fig. 9c), leading to the presence of easterly Jet at the middle-troposphere. These results confirm those obtained by the Walker circulation and, consequently, the pattern of rainfall anomalies.
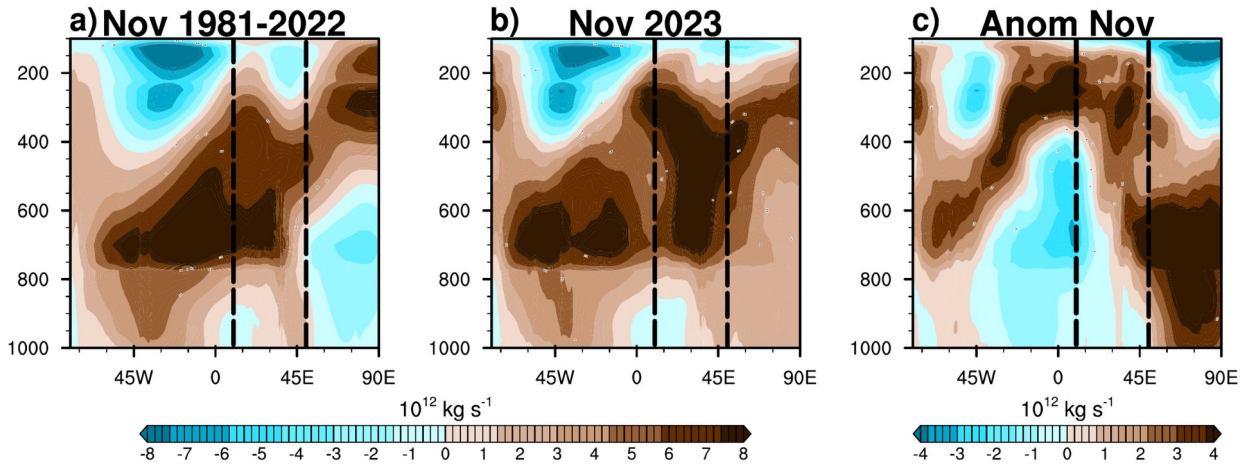
Fig 9: Zonal mass-weighted stream function (contours: 10^{11} kg s^{-1}) averaged between 10° S-10° N for (a) mean, (b) Nov. 2023 and (c) Nov. 2023 minus mean. Positive (negative) values indicate the westward (eastward) circulation. The dashed black lines denote the limits of EA.

4.2.2. Moisture flux divergence

Figure 10 shows the vertically integrated (1000-200 hPa) moisture flux convergence (color) and vertically integrated moisture flux (vectors). Positive values indicated convergence and negative values indicated divergence. Overall, the whole of EA exhibits moisture convergence with strong and significant moisture convergence in areas which feature strong and positive rainfall anomalies (Fig. 1c,f). The weak moisture divergence observed over the central part of DRC confirms the weak and negative rainfall anomalies also observed in this area. Note that all vectors in the EA region originate from the two neighbouring oceans through the western and eastern boundaries only. As for the western and eastern borders of the EA, we note a weakness of the meridional component along the northern and southern borders compared to the size of the zonal component. This confirms that these two oceans were mainly responsible for the wet episodes of 2023. The strong westerly winds become southwesterly to easterly, advecting moist air from the Atlantic Ocean towards the northern regions (Gabon, northern DRC, CAR and Cameroon). It is noteworthy that the strong westerly winds over the equatorial Atlantic originate from the NTA region, where strong and significant moisture divergence has been observed (not shown). For the eastern EA boundary, strong easterly winds from the Indian Ocean advect moist air in eastern and some southern regions, mainly over Somalia, southwest Ethiopia, eastern Kenya, Uganda and northern Angola. These results confirm the warm SST feature over oceans in Figure 2. Although the November 2023 DMI

is lower than in 2019 when the strongest positive IOD event since the 1950s occurred during October and November (Nicholson et al. 2022), the eastern region of EA was wetter in 2023 compared to 2019. This can be seen through the convergence and moisture flux anomalies, and consequently the higher precipitation in November 2023. One explanation could be the significant presence of the El Niño event in 2023, which contributed to humidifying the Eastern Africa region (Palmer et al. 2023; Roy and Troccoli 2024), unlike 2019, when during the positive IOD event, the El Niño episode was absent (Nicholson et al. 2022).
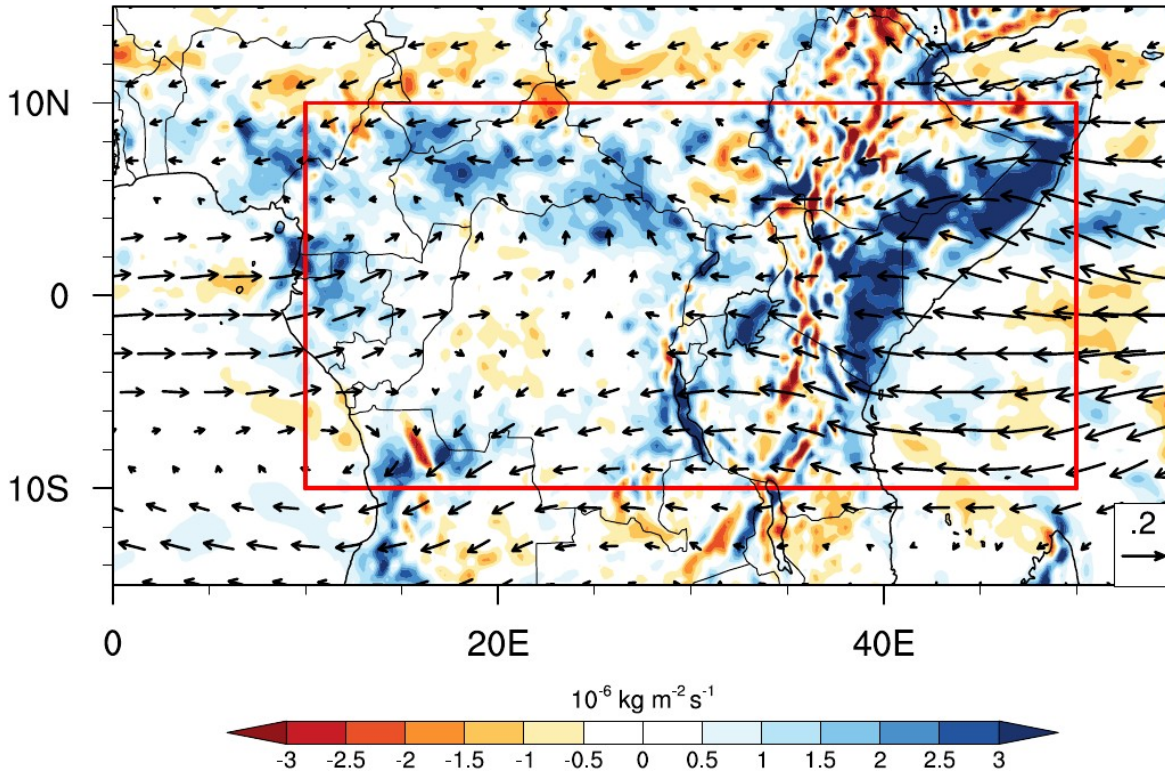
Fig 10: (a) Anomalies of vertically integrated (1000-200 hPa) moisture flux (vectors: kg m^{-1} s^{-1}) and vertically integrated moisture flux convergence (positive values) or divergence (negative values) anomalies (shading: 10^{-6} kg m^{-2} s^{-1}). Only significant vectors (shading) above the 90 % (95 %) level are shown. The red box indicates the EA region.

The northern regions (western Nigeria, northern Cameroon, southern Chad, CAR and South Sudan), which receive less than 2 mm day^{-1} of rainfall and have a near zero percentage contribution of November rainfall (Fig. 1a-b, d-e), recorded heavy rainfall in November 2023 (Fig. 1c-f). Similar to Nicholson et al. (2022) in October 2019, Figure 11a confirms this northward displacement of the state of the African rain band in November 2023. During this year, the 35 mm isopleth of the total column water vapor and the intertropical discontinuity (dashed blue and red lines respectively) move to the north, enhancing rainfall in the northern regions. These dashed lines correspond to the limit of the anomalous meridional mean sea level pressure gradient, characterised by anomalous

high pressure over the south of the 35 mm isopleth of the total column water vapor and the intertropical discontinuity lines, and lower over the north. Except over the Eastern EA areas. Similar pressure, intertropical discontinuity and 35 mm isopleth of the total column water vapor, and easterly (westerly) moisture flux anomaly were observed over Eastern EA (Gabon, CAR and Chad) in October (November) 2019 when extreme rainfall and flooding occurred in the latter country (Nicholson et al. 2022). As shown in Figure 11b, low-cloud cover (LCC) is below average in the southwest of EA (mainly over CB and south of Cameroon and Gabon) except in south-western CB and northern Angola (10°-20° E, 6°-10° S), but becomes above average over the northern part of EA (mainly over CAR) and the whole of East Africa. These positive LCC anomalies coincide with positive and strong surface net solar radiation anomalies. These spatial differences in atmospheric convective activity revealed by LCC and surface net solar radiation explain the spatial variations in rainfall anomalies shown in Fig. 1c,f.
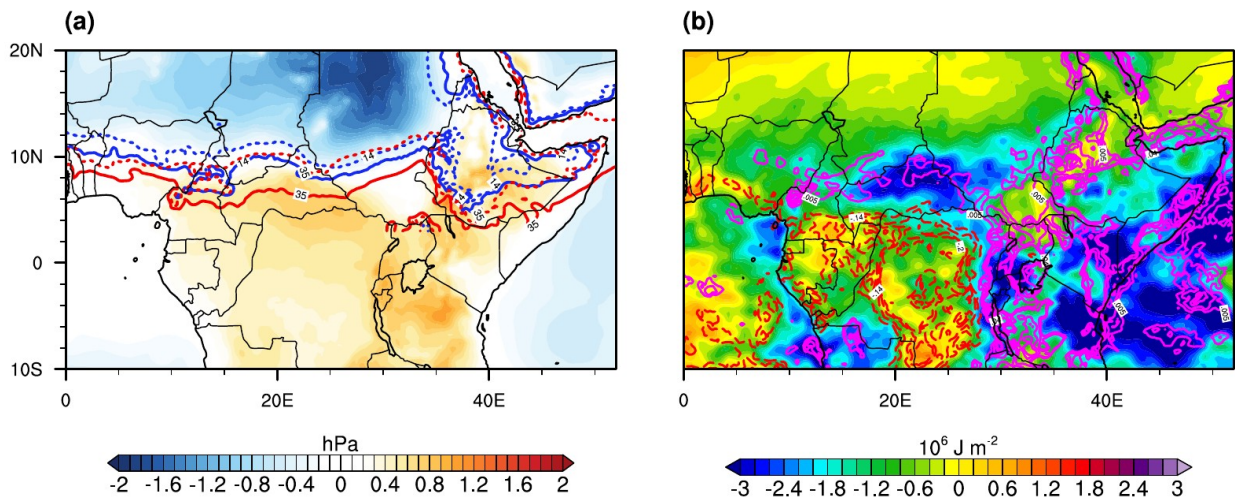
Fig 11: (a) The anomalous state of the African rain band in November 2023 is characterized by mean sea-level pressure anomalies (colored) relative to the 1981-2022 average, along with the positions of the intertropical discontinuity (ITD) and total column water vapor isopleths. The ITD is indicated by the 14°C 2-meter dew point temperature contours, with the mean ITD position shown by a solid blue line and the November 2023 position by a dashed blue line. Similarly, the mean location of the 35 mm total column water vapor isopleths is marked by a solid red line, while the November 2023 position is represented by a dashed red line. (b) Spatial representation of the surface net solar radiation anomalies (shading: 10^6 J m^{-2}). Red (Magenta) lines represent negative (positive) low cloud cover (%) anomalies.

4.2.3. LLWs, easterly Jets and MJO activity

One of the key atmospheric features over western EA are the African Easterly Jet (AEJ) and Tropical Easterly Jet (TEJ). Following Nicholson and Grist (2003), AEJ and TEJ are maximum easterly winds that occur at the mid-troposphere (from 700 to 600 hPa) and upper-troposphere (around 200 hPa) respectively. Here, we describe the characteristics of

these atmospheric features during the Nov 2023 extreme rainfall. The African Easterly Jet's southern component (AEJ-S) only appears from September to November and its jet core is located around 10° S in November (Kuete et al. 2022). In contrast to the AEJ-S, the northern component (AEJ-N) occurs during all months of the year, and its core is located around 5° N in November. As the AEJ-N, TEJ features during all months and is located near the south equator. Nicholson and Grist (2003) showed that Central Africa is a region where the divergence of the upper troposphere (Fig. 7a) is enhanced, which could favour convective activity (Fig. 8c), suggesting that the variability of the TEJ may influence the variability of precipitation in the region. Figure 12 shows Latitude/height cross-sections of easterly winds (dashed contours) of the 1981-2022 November mean and November 2023 at 10° E, overlaid by the zonal moisture flux (color) calculated from the West boundary (10° E) minus East boundary (30°E).

For the mean climatology (Fig. 12a), only AEJ-N is observed around 3°N at 700 hPa, with core speeds reaching 10 m s^{-1}. This intensification of AEJ-N coincides with strong moisture flux divergence. During November 2023 (Fig. 12b), both AEJ components and TEJ are present at the mid- and upper-troposphere respectively. During this year, the mid-level zonal moisture convergence (divergence) induced by the weak AEJ-S (jet core not exceeding 7 m s^{-1}; Kuete et al., 2019) increases (decreases), favouring increases mid-tropospheric moisture convergence south of the equator over western EA, resulting in wet conditions over the domain (Fig. 1c,f). AEJ-N moves further north and its intensity decreases from 10 m s^{-1} to 8 m s^{-1}, leading also to more western EA rainfall during positive IOD events, more pronounced during the October-November months (Moihamette et al. 2024). Following Moihamette et al. (2024), this decrease of the AEJ-N drove the equatorial easterly moisture transport to the western EA. These conclusions are in agreement with a study by Dezfuli and Nicholson (2013) showing that during October and November, the months with stronger (weaker) AEJ components experience dry (wet) conditions over western EA. Also, Nicholson and Grist (2003) showed that when both AEJ components are present, the western EA's rain-band moves further south (10° S to the equator), this is only observed during November. Another feature is the LLWs, which are weak in climatology, were anomalously strong and extended up to 700 hPa, mainly over southern-hemisphere latitudes. These wind changes lead to enhanced rainfall in western EA during the SON seasons (Pokam et al. 2014; Kuete et al. 2019; Taguela et al. 2022).
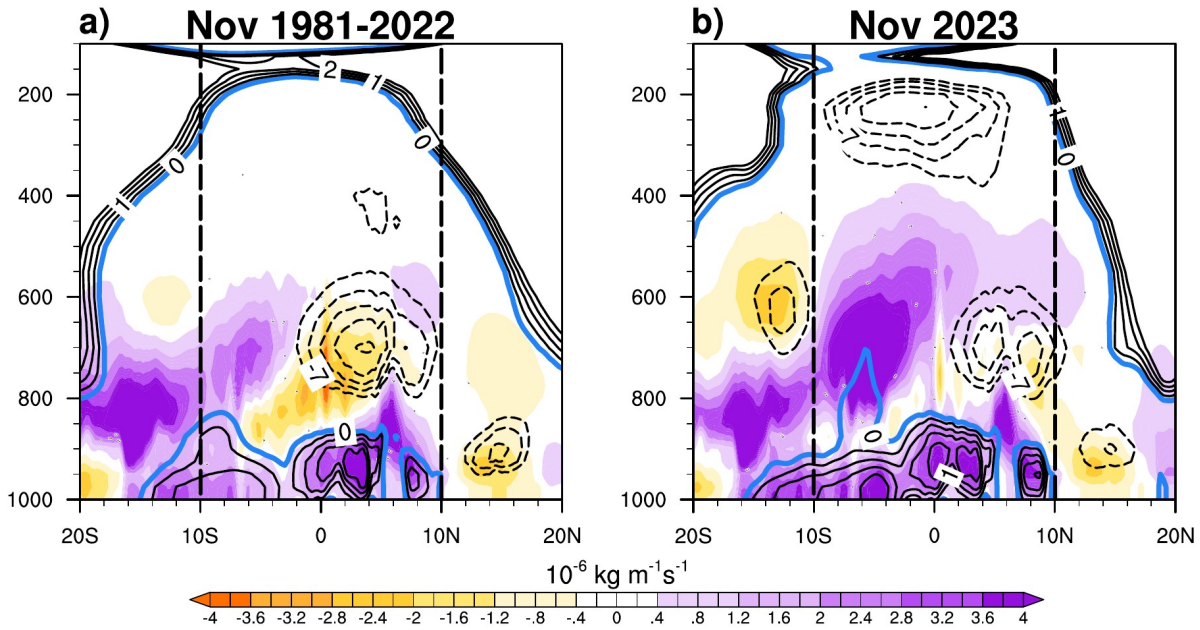
Fig 12: Latitude/height cross-sections of net zonal moisture flux (10^{-6} kg m^{-1} s^{-1}) calculated from West boundary (10° E) minus East boundary (30° E) for (a) climatology and (b) November 2023. Black solid (dashed) lines represent LLW (AEJ components and TEJ; U<-6 m s^{-1}) with the contour interval of 0.5 (1) m s^{-1}, calculated at 10° E for the respective periods. Positive values indicate moisture flux convergence, and negative values moisture flux divergence. The dashed black lines denote the limits of EA.

Here, we analyse one of eastern Africa's intra-seasonal climate drivers, the MJO, through the Real-time Multivariate MJO (RMM) index. This later strongly influences the equatorial Africa region's rainfall during March-April-May (Sandjon et al. 2012) and November and December (Pohl and Camberlin 2006; Berhane and Zaitchik 2014; Berhane 2016; Zaitchik 2017; Palmer et al. 2023). According to Pohl and Camberlin (2006) and Kimani et al. (2020), during phases 6-8 (1-4) of the MJO, there is an increased chance of the highest rainfall over the coastal (highlands) regions of East Africa during OND months, through moisture advection from the Indian Ocean. The ENSO-MJO relationship was studied by Pohl and Matthews (2007), who found that maximum MJO activity is often observed during El-Niño events. In addition, Berhane (2016) showed that this juxtaposition of MJO activity and ENSO events leads to an increase in precipitation that is greater than when El-Nino events are absent.
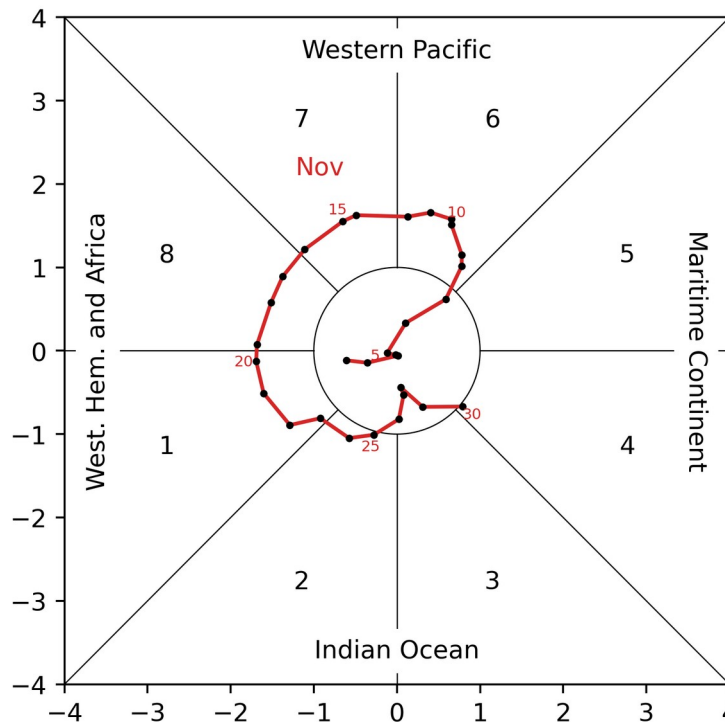
Fig 13: Madden-Julian Oscillation (MJO) phases and intensity (red line) space diagram for November 2023. Each black dot represents the value for a given day with select dates labelled in red. [Source: NOAA/NCEI Climate.gov, https://www.ncei.noaa.gov/access/monitoring/monthly-report/synoptic/ 202311, accessed 26/11/24]

Figure 13 shows the MJO phase space diagram for November 2023, based on the RMM index. It should be noted that the MJO was active for 19 days, during phases leading to wet periods in the highlands and coastal areas of East Africa (Pohl and Camberlin 2006; Berhane and Zaitchik 2014; Zaitchik 2017). During November 2023, the MJO was in phases 6-8 from 8 to 19 November, which are the phases leading to wet spells over the East African coast (Pohl and Camberlin 2006; Zaitchik 2017), mainly over Somalia and the eastern parts of Ethiopia, Tanzania and Kenya regions. Also, during 20-25 and 30 November 2023, the MJO was in phases 1, 2 and 4, which are the phases typically associated with increased rainfall over the Highland region of East Africa (Pohl and Camberlin 2006), mainly over Uganda, the western and northern part of Kenya and Tanzania, respectively.

5. Summary and Conclusions

This study examines the extreme wet conditions that occurred in November 2023 in Equatorial Africa (EA) and shows that this rainy episode was caused by several factors. While some anomalous rainfall over both western and eastern equatorial Africa were attributed to moisture transport from the Atlantic and Indian oceans respectively, the unusually very strong November 2023 MJO activity was a significant factor. In addition to meteorological conditions, further research is therefore needed to quantify the roles that

642 dynamic and thermodynamic processes played in the extreme events of November 2023.
643 The most important findings of this study are as follows:

644   - Although the rain band in November is over the south equator, many north
645   areas feature positive rainfall anomalies, most pronounced over eastern
646   Africa. These strongest November 2023 rainfall anomalies occur when
647   significant SST anomalies were observed in the three equatorial oceans.

648   - In contrast to the extreme rainfall of November 2019 in East Africa, where
649   the DMI reached record levels, the DMI of November 2023, which is lower
650   than that of 2019, is causing more rainfall. This may be due to the presence
651   of strong El Nino conditions over the equatorial Pacific in 2023. But over
652   central Africa, the rainfall anomalies in 2023 are lower than in 2019,
653   certainly due to the state of the equatorial Atlantic Ocean, which was
654   warmer in 2019 than in 2023.

655   - SST anomalies over the Atlantic (Indian) Ocean are associated with
656   anomalous westerly (easterly) winds that bring more moisture over EA (Fig.
657   5c). Moisture flux from both oceans, respectively (Fig. 5f), induced a
658   weakening of the ascending and descending branches of both neighboring
659   oceans Walker-like cells (Figs. 8 and 9).

660   - The westerly moisture flux from the Atlantic Ocean that veered into
661   southwesterlies moved the rainbelt further north by enhancing the
662   transport of moist air over the northern (5°-10° N) regions (Fig. 11).

663   - Over western EA where extreme rain also occurs, the African wind and
664   easterly wind regime is an important factor. The presence of strong
665   equatorial westerlies, AEJ-S and TEJ, and the movement of AEJ-N further
666   north have also retarded the retreat of the West African rain band, causing
667   positive rainfall anomalies over northern areas (especially over Nigeria,
668   Cameroon, CAR, Sudan and South Chad).

669   - Another driver is the MJO activity, which was active during several days of
670   November 2023 (Fig. 12). We have shown that the positive rainfall anomalies
671   over East Africa coincided with active phases of MJO, which enhanced
672   rainfall in November over both western and eastern areas of East Africa.
673   This increase in rainfall was significant with the occurrence of the El-Niño
674   events.

675   This study demonstrates that the anomalous wetness conditions over Equatorial
676 Africa were caused mainly by the Atlantic and Indian oceans, through the anomalous
677 moisture transport and moisture flux divergence, Walker circulation, and changes in the
678 zonal winds, induced by extremely strong SST anomalies. These anomalous patterns were
679 similar to those observed over this region in October/November 2019 when extreme
680 rainfall occurred, following Nicholson et al. (2021). The present study demonstrates the
681 importance of accounting for ocean-atmosphere interactions in intra-seasonal forecast

682   models to refine regional climate information provided to policymakers. It is important to
683   highlight that the robustness of these findings requires additional evaluation. Our study
684   exclusively examines the meteorological causes of these extreme events. Further
685   investigations should encompass the roles that dynamic and thermodynamic processes
686   played in these November 2023 events.

687
688
689
690
691
692
693
694
695
696
697
698
699
700
701
702
703
704
705
706
707
708
709
710
711
712
713
714
715
716
717
718
719
720

Code availability Figures shown in this study are plotted using the NCAR Command Language (NCL; https://doi.org/10.5065/D6WD3XH5, NCAR Command Language, 2017). Codes can be obtained from the corresponding author.

Data Availability Statement All observational and reanalysis data used in this study are publicly available at no charge and with unrestricted access. One plot is generated using the web site of NOAA/NCEI, at https://www.ncei.noaa.gov/. The ERA5 reanalysis is produced within the Copernicus Climate Change Service (C3S) by the ECMWF and is accessible via the link https://cds.climate.copernicus.eu/datasets/reanalysis-era5-pressure-levels-monthly-means?tab=download; the CHIRPS2 data are available at https://data.chc.ucsb.edu/products/CHIRPS-2.0/global_daily/netcdf/; the ERSST data are available at https://iridl.ldeo.columbia.edu/SOURCES/.NOAA/.NCDC/.ERSST/.version5/.

Author's contributions
HNN: Conceptualization; data upload; data analysis; formal analysis; investigation; methodology; software; validation; writing-original draft; writing-review and editing. **MG:** Project administration; supervision; formal analysis; investigation; validation; writing-original draft; writing-review and editing. **RST:** Project administration; supervision; validation; methodology; writing; review and editing. **ATT:** Project administration; validation; methodology; writing; review and editing. **DAV:** Project administration; supervision; validation, methodology; writing; review and editing.

Conflict of Interest The authors declare no conflicts of interest relevant to this study.

Funding Not applicable

Acknowledgements The authors thank you to all reanalysis, observational and satellite data providers used in this study. We would like to express our gratitude to the anonymous reviewers, along with the editor for their constructive suggestions, which have greatly improved the quality of the paper. We gratefully appreciate the efforts of the International Joint Laboratory Dynamics of Terrestrial Ecosystems in Central Africa (IJL DYCOCA/ LMI DYCOFAC) initiative during the realisation of this work.

References

Berhane, F. and Zaitchik, B.: Modulation of daily precipitation over East Africa by the madden–julian oscillation, J. Climate, 27, 6016–6034, https://doi.org/10.1175/jcli-d-13-00693.1, 2014

Berhane, F.: Intraseasonal Precipitation Variability Over Tropical Africa, Ph.D.,Johns Hopkins University, Baltimore, MD, USA, 2016

Chadwick, R., Good, P., and Willett, K.: A simple moisture advection model of specific humidity change over land in response to SST warming, J. Climate, 29, 7613–7632, https://doi.org/10.1175/jcli-d-16-0241.1, 2016

Chobo, J. S. and Huo, L.: The relationship between extreme precipitation events in East Africa during the short rainy season and Indian Ocean Sea surface temperature, , J. Geosc. Env. Prot., 12, 1–16, https://doi.org/10.4236/gep.2024.129001, 2024

Dezfuli, A. K. and Nicholson, S. E.: The relationship of rainfall variability in Western Equatorial Africa to the tropical oceans and atmospheric circulation. Part II: The Boreal Autumn, J. Climate, 26, 66–84, https://doi.org/10.1175/jcli-d-11-00686.1, 2013

Fotso-Nguemo, T. C., Diallo, I., Diakhaté, M., Vondou, D. A., Mbaye, M. L., Haensler, A., Gaye, A. T., and Tchawoua, C.: Projected changes in the seasonal cycle of extreme rainfall events from CORDEX simulations over Central Africa, Climatic Change, 155, 339–357, https://doi.org/10.1007/s10584-019-02492-9, 2019

Funk, C., Dettinger, M. D., Michaelsen, J. C., Verdin, J. P., Brown, M. E., Barlow, M., and Hoell, A.: Warming of the Indian Ocean threatens eastern and southern African food security but could be mitigated by agricultural development, Proc. Nat. Acad. Sci. USA, 105, 11081–11086, https://doi.org/10.1073/pnas.0708196105, 2008

Gudoshava, M., Misiani, H. O., Segele, Z. T., Jain, S., Ouma, J. O., Otieno, G., Anyah, R., Indasi, V. S., Endris, H. S., Osima, S., Lennard, C., Zaroug, M., Mwangi, E., Nimusiima, A., Kondowe, A., Ogwang, B., Artan, G., and Atheru, Z.: Projected effects of 1.5 °C and 2 °C global warming levels on the intra-seasonal rainfall characteristics over the Greater Horn of Africa, Environ. Res. Lett., 15, 034037, https://doi.org/10.1088/1748-9326/ab6b33, 2020

Gudoshava, M., Nyinguro, P., Talib, J., Wainwright, C., Mwanthi, A., Hirons, L., de Andrade, F., Mutemi, J., Gitau, W., Thompson, E., Gacheru, J., Marsham, J., Endris, H. S., Woolnough, S., Segele, Z., Atheru, Z., and Artan, G.: Drivers of sub-seasonal extreme rainfall and their representation in ECMWF forecasts during the Eastern African March-to-May seasons of 2018–2020, Meterol. Appl., 31, https://doi.org/10.1002/met.70000, 2024

Hastenrath, S., Polzin, D., and Mutai, C.: Diagnosing the droughts and floods in Equatorial East Africa during boreal autumn 2005–08, J. Climate, 23, 813–817, https://doi.org/10.1175/2009jcli3094.1, 2010

Hastenrath, S., Polzin, D., and Mutai, C.: Circulation mechanisms of Kenya rainfall anomalies, J. Climate, 24, 404–412, https://doi.org/10.1175/2010jcli3599.1, 2011

Herrnegger, M., Kray, P., Stecher, G., Cherono Kiplangat, N., Otieno, D., Olang, L., and Nicholson, S. E.: Paleohydrology repeating? Regional hydrological change may lead to an overflow and cross-mixing of an alkaline and a freshwater lake in East Africa, J. Hydrol., 55, 101951, https://doi.org/10.1016/j.ejrh.2024.101951, 2024

Ibebuchi, C. C.: Revisiting the 1992 severe drought episode in South Africa: The role of El Niño in the anomalies of atmospheric circulation types in Africa south of the equator, Theor. Appl. Climatol., 146, 723–740, https://doi.org/10.1007/s00704-021-03741-7, 2021

Indeje, M., Semazzi, F. H. M., and Ogallo, L. J.: ENSO signals in East African rainfall seasons, Int. J. Climatol., 20, 19–46, https://doi.org/10.1002/(sici)1097-0088(200001)20:1<19::aid-joc449>3.0.co;2-0, 2000

Ingeri, C., Wen, W., Sebaziga, J. N., Iyakaremye, V., Ekwacu, S., Ayabagabo, P., Twahirwa, A., and Kazora, J.: Potential driving systems associated with extreme rainfall across East Africa during october to december (OND) season 2019, J. Geosc. Env. Prot., 12, 25–49, https://doi.org/10.4236/gep.2024.127003, 2024

Kenfack, K., Marra, F., Djomou, Z. Y., Tchotchou, L. A. D., Tamoffo, A. T., and Vondou, D. A.: Dynamic and thermodynamic contribution to the October 2019 exceptional rainfall in western central Africa, Weather Clim. Dynam., 5, 1457–1472, https://doi.org/10.5194/wcd-5-1457-2024, 2024

Kilavi, M., MacLeod, D., Ambani, M., Robbins, J., Dankers, R., Graham, R., Titley, H., Salih, A., and Todd, M.: Extreme rainfall and flooding over central kenya including nairobi city during the long-rains season 2018: Causes, predictability, and potential for early warning and actions, Atmosphere, 9, 472, https://doi.org/10.3390/atmos9120472, 2018

Kimani, M., Hoedjes, J. C. B., and Su, Z.: An assessment of MJO circulation influence on air–sea interactions for improved seasonal rainfall predictions over East Africa, J. Climate, 33, 8367–8379, https://doi.org/10.1175/jcli-d-19-0296.1, 2020

Kuete, G., Mba, W. P., James, R., Dyer, E., Annor, T., and Washington, R.: How do coupled models represent the African Easterly Jets and their associated dynamics over Central Africa during the September–November rainy season? Clim. Dynam., 60, 2907–2929, https://doi.org/10.1007/s00382-022-06467-y, 2022

Kuete, G., Pokam Mba, W., and Washington, R.: African Easterly Jet South: Control, maintenance mechanisms and link with Southern subtropical waves, Clim. Dynam., 54, 1539–1552, https://doi.org/10.1007/s00382-019-05072-w, 2019

Li, C., Chai, Y., Yang, L., and Li, H.: Spatio-temporal distribution of flood disasters and analysis of influencing factors in Africa, Nat. Hazards, 82, 721–731, https://doi.org/10.1007/s11069-016-2181-8, 2016

Longandjo, G.-N. T., and Rouault, M.: On the structure of the regional-scale circulation over Central Africa: Seasonal evolution, variability, and mechanisms, J. Climate, 33, 145–162, https://doi.org/10.1175/jcli-d-19-0176.1, 2020

Longandjo, G.-N. T., and Rouault, M.: Revisiting the seasonal cycle of rainfall over Central Africa, J. Climate, 37(3), 1015–1032, https://doi.org/10.1175/jcli-d-23-0281.1, 2024

Lüdecke, H.-J., Müller-Plath, G., Wallace, M. G., and Lüning, S.: Decadal and multidecadal natural variability of African rainfall, J. Hydrol., 34, 100795, https://doi.org/10.1016/j.ejrh.2021.100795, 2021

Lutz, K., Jacobeit, J., and Rathmann, J.: Atlantic warm and cold water events and impact on African west coast precipitation, Int. J. Climatol., 35, 128–141, https://doi.org/10.1002/joc.3969, 2014

Madden, R. A., and Julian, P. R.: Detection of a 40–50 day oscillation in the zonal wind in

850   the Tropical Pacific, J. Atmos. Sci., 28, 702–708, https://doi.org/10.1175/1520-
851   0469(1971)028<0702:doadoi>2.0.co;2, 1971

852 Madden, R. A., and Julian, P. R.: Description of global-scale circulation cells in the Tropics
853   with a 40–50 day period, J. Atmos. Sci., 29, 1109–1123,
854   https://doi.org/10.1175/1520-0469(1972)029<1109:dogscc>2.0.co;2, 1972

855 McHugh, M. J., and Rogers, J. C.: North atlantic oscillation influence on precipitation
856   variability around the southeast african convergence zone, J. Climate, 14, 3631–
857   3642, https://doi.org/10.1175/1520-0442(2001)014<3631:naoiop>2.0.co;2, 2001

858 Moihamette, F., Pokam, W. M., Diallo, I., & Washington, R.: Extreme Indian Ocean dipole
859   and rainfall variability over Central Africa, Int. J. Climatol., 42, 5255–5272,
860   https://doi.org/10.1002/joc.7531, 2022

861 Moihamette, F., Pokam, W. M., Diallo, I., and Washington, R.: Response of regional
862   circulation features to the Indian Ocean dipole and influence on Central Africa
863   climate, Clim. Dynam., 62, 1–21, https://doi.org/10.1007/s00382-024-07251-w, 2024

864 Nana, H. N., Tamoffo, A. T., Kaissassou, S., Djiotang Tchotchou, L. A., Tanessong, R. S.,
865   Kamsu-Tamo, P. H., Kenfack, K., and Vondou, D. A.: Performance-based evaluation
866   of NMME and C3S models in forecasting the June–August Central African rainfall
867   under the influence of the South Atlantic Ocean Dipole, Int. J. Climatol., 44, 2462–
868   2483, https://doi.org/10.1002/joc.8463, 2024

869 Nana, H. N., Tanessong, R. S., Tchotchou, L. A. D., Tamoffo, A. T., Moihamette, F., and
870   Vondou, D. A.: Influence of strong South Atlantic Ocean Dipole on the Central
871   African rainfall's system, Clim. Dynam., 62, 1–16, https://doi.org/10.1007/s00382-
872   023-06892-7, 2023

873 Ngavom, Z., Fotso-Nguemo, T. C., Vondou, D. A., Fotso-Kamga, G., Zebaze, S., Yepdo, Z. D.,
874   and Diedhiou, A.: Projected changes in population exposure to extreme
875   precipitation events over Central Africa under the global warming levels of 1.5 °C
876   and 2 °C: Insights from CMIP6 simulations, Model. Earth Syst. Environ., 10, 5753–
877   5769, https://doi.org/10.1007/s40808-024-02091-3, 2024

878 Nicholson, S. E.: Long-term variability of the East African 'short rains' and its links to large-
879   scale factors, Int. J. Climatol., 35, 3979–3990, https://doi.org/10.1002/joc.4259, 2015

880 Nicholson, S. E., Fink, A. H., Funk, C., Klotter, D. A., and Satheesh, A. R.: Meteorological
881   causes of the catastrophic rains of October/November 2019 in equatorial Africa,
882   Global. Planet. Change, 208, 103687,
883   https://doi.org/10.1016/j.gloplacha.2021.103687, 2022

884 Nicholson, S. E., and Grist, J. P.: The seasonal evolution of the atmospheric circulation over
885   West Africa and Equatorial Africa, J. Climate, 16, 1013–1030,
886   https://doi.org/10.1175/1520-0442(2003)016<1013:tseota>2.0.co;2, 2003

887 Onyutha, C.: Geospatial trends and decadal anomalies in extreme rainfall over uganda,
888   east africa, Adv. Meteorol., 2016, 1–15, https://doi.org/10.1155/2016/6935912, 2016

889 Palmer, P. I., Wainwright, C. M., Dong, B., Maidment, R. I., Wheeler, K. G., Gedney, N.,
890   Hickman, J. E., Madani, N., Folwell, S. S., Abdo, G., Allan, R. P., Black, E. C. L., Feng, L.,
891   Gudoshava, M., Haines, K., Huntingford, C., Kilavi, M., Lunt, M. F., Shaaban, A., and
892   Turner, A. G.: Drivers and impacts of Eastern African rainfall variability, Nat. Rev.
893   Earth Environ., 4, 254–270, https://doi.org/10.1038/s43017-023-00397-x, 2023

894 Pohl, B., and Camberlin, P.: Influence of the Madden–Julian Oscillation on East African
895   rainfall. I: Intraseasonal variability and regional dependency, Quart. J. Roy.

896   Meteorol. Soc., 132, 2521–2539, https://doi.org/10.1256/qj.05.104, 2006

897 Pohl, B., and Matthews, A. J.: Observed changes in the lifetime and amplitude of the
898   madden–julian oscillation associated with interannual ENSO sea surface
899   temperature anomalies, J. Climate, 20, 2659–2674,
900   https://doi.org/10.1175/jcli4230.1, 2007

901 Pokam, W. M., Bain, C. L., Chadwick, R. S., Graham, R., Sonwa, D. J., and Kamga, F. M.:
902   Identification of processes driving low-level westerlies in west equatorial africa, J.
903   Climate, 27, 4245–4262, https://doi.org/10.1175/jcli-d-13-00490.1, 2014

904 Pokam, W. M., Djiotang, L. A. T., and Mkankam, F. K.: Atmospheric water vapor transport
905   and recycling in Equatorial Central Africa through NCEP/NCAR reanalysis data,
906   Clim. Dynam., 38, 1715–1729, https://doi.org/10.1007/s00382-011-1242-7, 2011

907 Roy, I., and Troccoli, A.: Identifying important drivers of East African October to December
908   rainfall season, Sci. Tot. Env., 914, 169615,
909   https://doi.org/10.1016/j.scitotenv.2023.169615, 2024

910 Sandjon, A. T., Nzeukou, A., and Tchawoua, C.: Intraseasonal atmospheric variability and
911   its interannual modulation in Central Africa, Meteorol. Atmos. Phys., 117, 167–179.
912   https://doi.org/10.1007/s00703-012-0196-6, 2012

913 Seager, R., Naik, N., and Vecchi, G. A.: Thermodynamic and dynamic mechanisms for
914   large-scale changes in the hydrological cycle in response to global warming*, J.
915   Climate, 23, 4651–4668, https://doi.org/10.1175/2010jcli3655.1, 2010

916 Shisanya, Chris A.: The 1983-1984 drought in Kenya, J. East. Afr. Res. Dev., 20, 127–148,
917   http://www.jstor.org/stable/24326214, 1990

918 Stachnik, J. P., and Schumacher, C.: A comparison of the Hadley circulation in modern
919   reanalyses, J. Geophys Res-Atmos., 116, n/a-n/a,
920   https://doi.org/10.1029/2011jd016677, 2011

921 Taguela, T. N., Pokam, W. M., Dyer, E., James, R., and Washington, R.: Low-level circulation
922   over Central Equatorial Africa as simulated from CMIP5 to CMIP6 models, Clim.
923   Dynam., 62, 8333–8351, https://doi.org/10.1007/s00382-022-06411-0, 2022

924 Tamoffo, A. T., Amekudzi, L. K., Weber, T., Vondou, D. A., Yamba, E. I., and Jacob, D.:
925   Mechanisms of rainfall biases in two CORDEX-CORE regional climate models at
926   rainfall peaks over central equatorial africa, J. Climate, 35, 639–668,
927   https://doi.org/10.1175/jcli-d-21-0487.1, 2022

928 Tamoffo, A. T., Weber, T., Abel, D., Ziegler, K., Cabos, W., Sein, D. V., and Laux, P.:
929   Regionally coupled climate model ROM projects more plausible precipitation
930   change over Central Equatorial Africa, J. Geophys Res-Atmos., 129,
931   https://doi.org/10.1029/2024jd041466, 2024

932 Tanessong, R. S., Vondou, D. A., Djomou, Z. Y., and Igri, P. M.: WRF high resolution
933   simulation of an extreme rainfall event over Douala (Cameroon): A case study,
934   Model. Earth Syst. Environ., 3, 927–942, https://doi.org/10.1007/s40808-017-0343-7,
935   2017

936 Wahiduzzaman, M., and Luo, J.-J.: A statistical analysis on the contribution of El Niño–
937   Southern Oscillation to the rainfall and temperature over Bangladesh, Meteorol.
938   Atmos. Phys., 133, 55–68, https://doi.org/10.1007/s00703-020-00733-6, 2020

939 Wainwright, C. M., Finney, D. L., Kilavi, M., Black, E., and Marsham, J. H.: Extreme rainfall in
940   East Africa, October 2019–January 2020 and context under future climate change,
941   Weather, 76, 26–31, https://doi.org/10.1002/wea.3824, 2020

942 Yao, L., Lu, J., Xia, X., Jing, W., and Liu, Y.: Evaluation of the ERA5 sea surface temperature
943   around the Pacific and the Atlantic, IEEE Access, 9, 12067–12073,
944   https://doi.org/10.1109/access.2021.3051642, 2021
945 Zaitchik, B. F.: Madden-Julian Oscillation impacts on tropical African precipitation, Atmos.
946   Res., 184, 88–102, https://doi.org/10.1016/j.atmosres.2016.10.002, 2017
947 Zheng, X., and Eltahir, E. A. B.: A Soil Moisture–Rainfall Feedback Mechanism: 2. Numerical
948   experiments, Water Resour. Res., 34, 777–785, https://doi.org/10.1029/97wr03497,
949   1998